Massive MIMO Channel Measurements for a Railway Station Scenario

Markus Hofer, David Löschenbrand, Stefan Zelenbaba, Gerhard Humer,
Benjamin Rainer and Thomas Zemen

Security & Communication Technologies, AIT Austrian Institute of Technology GmbH, Austria
Email: markus.hofer@ait.ac.at

***Abstract*—In this paper we present dual-band massive multiple-input multiple-output (MIMO) channel measurements for a railway station scenario. The massive MIMO link shall provide an ultra-reliable low-latency communication link from the control center to the locomotive. In this measurement campaign the locomotive moves from line-of-sight to non line-of-sight. We present dual frequency band measurements, where the massive MIMO array at the base station has 24 receive antenna elements at 1890 MHz and 8 receive antenna elements at 748 MHz. The measurement bandwidth is 20 MHz and we use a repetition rate of 1 ms to acquire the time-variant channel frequency response from the locomotive to all 32 antenna elements in parallel. In this paper, we provide a first analysis of the root mean square delay spread, the path loss coefficients and the channel hardening in both frequency bands.**

***Index Terms*—multiband, massive MIMO, railway**

I. Introduction

Reliable wireless communication systems are a key component for improving efficiency and safety for future automated train operation and cost-effective regional railways. Low-latency and highly reliable wireless train-to-infrastructure (T2I) and train-to-train (T2T) communication are required to ensure the real-time exchange of kinematic data (highly accurate position, speed, etc.) between locomotives as well as between the central signaling system and locomotives. However, the communication link quality can be severely degraded as the propagation conditions between moving locomotives change rapidly and the path of direct visibility is often blocked by buildings or other objects. In favorable propagation scenarios, massive multiple-input multiple-output (MIMO) mitigates random wireless channel fluctuations (fading) serving ultra-reliable and low latency communication (URLLC) use cases, however, the explicit knowledge, in which railway scenarios favorable conditions are available is unknown.

In [1] Unterhuber et al. show T2T measurements for different high speed train scenarios. The authors analyze the path loss coefficient and stationary region length for single-input single-output (SISO) measurements. In [2]–[4] further high speed railway channel measurements are shown. The authors of [5] show quasi-static mmWave massive MIMO channel measurements at 28 GHz in a high speed railway station and analyse path loss and delay spread. Massive MIMO measurements for mobile railway scenarios have not yet been discussed in literature.

Scientific contribution:

- In this paper we present simultaneous massive MIMO measurements for a railway station scenario at two carrier frequencies for a transition from line-of-sight (LOS) to non-line of sight (NLOS)
- We evaluate the path loss coefficient, root mean square (RMS) delay spread and channel hardening.

II. Measurement Campaign

A. Scenario Description

We conduct massive MIMO channel measurements at an urban railway station in Sigmundsherberg, Austria, shown in Fig. 1. The railway station has two platforms with multiple tracks. The platforms are connected via a footbridge as indicated in the figure, where the massive MIMO arrays are mounted. The railway station is surrounded by several buildings in the north, and a railway museum is located in the west. A locomotive, equipped with an omni-directional transmit antenna, moves from the footbridge with LOS to the west behind the museum to NLOS. The maximum traveled distance is about 900 m with a maximum velocity of about 40 km/h. In a second measurement run the locomotive moves from west to the east, back to the footbridge. We repeat the measurements in total eight times, four times in each direction.

B. Antenna Design

32 custom built patch antennas over a finite ground plane are utilized as receive antennas. The patch element size is $0.25\,\lambda$ and they are spaced $0.5\,\lambda$ horizontally and vertically in both frequency bands. The antennas for 1890 MHz are arranged in a $12{\times}2$ uniform linear array (ULA), for 748 MHz they are arranged in a $4{\times}2$ ULA, as shown in Fig. 2. Filters are used to suppress strong signals in adjacent frequency bands from nearby base stations. The printed circuit board (PCB) material is standard FR4. For additional frequency filtering, its thickness of 0.5 mm (1890 MHz) and 1.5 mm (748 MHz) is chosen as small as possible to still achieve the desired bandwidth of $2\,\%$ of the respective sounding frequency. A LAIRD TRA6927M3 omni-directional antenna is used as transmit antenna for both frequency bands and mounted in

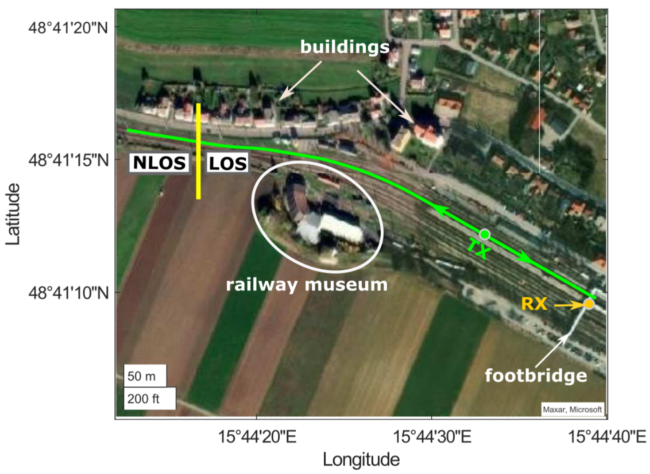

Fig. 1. Satellite view of Sigmundsherberg.

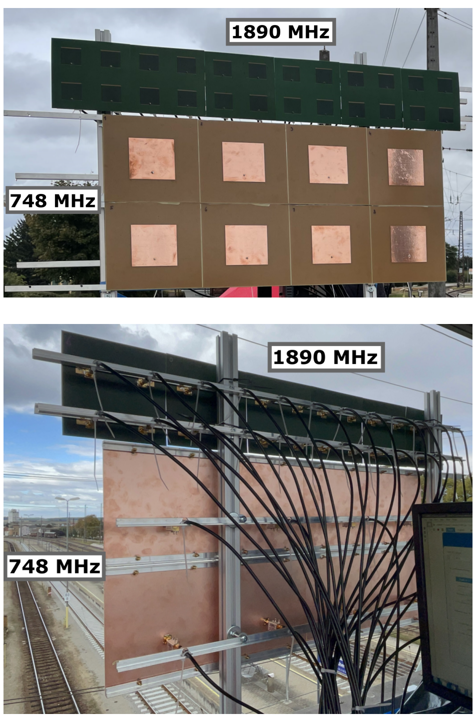

Fig. 2. Front and back view of custom made receive antenna arrays.

the middle of the roof top of the locomotive, as shown in Fig. 3.

C. Sounding Signal

A complex baseband multitone signal is used to measure the time-variant channel characteristics [6]–[8]. The multitone signal consists of $Q = 80$ subcarriers. We choose a subcarrier spacing of $\Delta f = 1/T = 250\,\text{kHz}$, with T the period of the sounding signal, such that we achieve a maximum excess delay of $\tau_{\text{max}} = 4\,\mu\text{s}$. This leads to a sounding bandwidth of 20 MHz. A raised cosine filter with roll-off factor 0.3 is used to reduce out of band emissions to avoid interference in neighbouring bands.

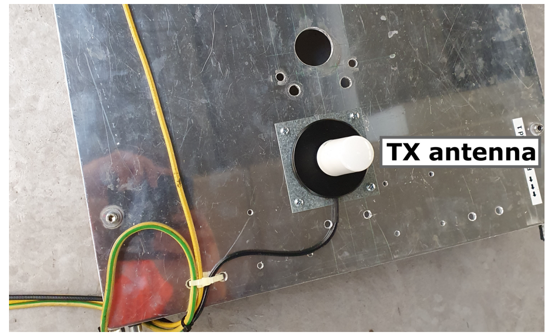

Fig. 3. Transmit antenna mounted at the roof top of locomotive

We use the method of [9] to obtain a multitone signal with a crest factor of 1.36 (see [7] for more details). The sounding signal is constructed by concatenating three repetitions of the multitone signal. This leads to a total sounding signal length of $3T = 12\,\mu\text{s}$. We use the first period T of the sounding signal as cyclic prefix (CP) (see [6]–[8] for more details).

Each individual antenna $a \in \{1, \ldots, A\}$, $A = 32$, receives the sounding signal multiplied with the propagation channel $H_a[m,q]$ resulting in $Y_a[m,q] = H_a[m,q]X[q] + n[m,q]$, where m denotes the time index and q the subcarrier index, $X[q]$ the known sounding signal and $n[m,q]$ the noise. Please note that antennas 1 to 24 operate at a center frequency of 1890 MHz and antennas 25 to 32 operate at a center frequency of 748 MHz. Since the sounding signal $X[q]$ is known at the receiver (RX), the calibrated channel transfer function is obtained by dividing the received sounding signal in the frequency domain by the known sounding signal, i.e., [7], [10]

$$\hat{H}_a[m,q] = \frac{Y_a[m,q]}{X[q]\hat{H}_a^{\text{RF}}[q]}. \tag{1}$$

The calibration transfer function $\hat{H}_a^{\text{RF}}[m,q]$ is obtained by a calibration phase prior to the measurement. The same measurement principle is used for both frequency bands. The sounding is performed at regular time intervals of $T_{\text{R}} = 1\,\text{ms}$. This allows a Doppler estimation up to a relative velocity of $v_{\text{max}} = c_0 f_{\text{Dmax}}/f_{\text{c}} = c_0/2T_{\text{R}} f_{\text{c}} = 79.37\,\text{m/s}$, where c_0 is the speed of light in air, f_{c} is the carrier frequency of the highest frequency band, and $f_{\text{Dmax}} = 1/(2T_{\text{R}})$.

D. GPS and Synchronization

At transmitter (TX) and RX, Precision Test Systems GPS10eR [11] Rubidium clocks provide a 10 MHz reference signal with low phase noise and a pulse per second (PPS) signal for timing synchronization between TX and RX. Before the measurement starts, the RX Rubidium clock is connected via coaxial cables to the TX Rubidium clock and synchronized to it. The TX Rubidium clock acts as primary clock source.

The GPS position is tracked and recorded with an inertial measurement unit (IMU) with an update rate of 500 Hz, which allows for an accurate position tracking of the locomotive.

Start and stop time of the measurement are recorded using GPS time tags.

III. Measurement Evaluation

A. Local Scattering Function, Power Delay Profile and Delay Spread

We use the local scattering function (LSF) [6], [12]–[14] for measurement data evaluation. With the time-variant frequency response $\hat{H}_a[m,q]$, the estimate of the LSF is given by

$$\hat{\mathcal{C}}_a[l;n,p] = \frac{1}{IJ}\sum_{w=0}^{IJ-1}\left|\mathcal{H}_a^{(G_w)}[l;n,p]\right|^2, \tag{2}$$

with the Doppler index $p \in \{-M/2\ldots,M/2-1\}$, the delay index $n \in \{0,\ldots,Q-1\}$ and the stationarity region index l. The delay resolution is defined by $\tau_\mathrm{s} = 1/Q\Delta f$. The tapered frequency response is

$$\mathcal{H}_a^{(G_w)}[l;n,p] = \sum_{m=-M/2}^{M/2-1}\sum_{q=-(Q-1)/2}^{(Q-1)/2}\hat{H}_a[m+Ml,q] \cdot G_w[m,q]\mathrm{e}^{-\mathrm{j}2\pi(pm-nq)}, \tag{3}$$

where the tapers $G_w[m,q]$ are two-dimensional discrete prolate spheroidal (DPS) sequences as shown in detail in [12], [15]. The number of tapers in the time and frequency domain is set to $I=2$ and $J=1$, respectively [12], [16].

We choose $M=100$, which corresponds to a stationarity region length of 100 ms. We calculate the power delay profile (PDP) from the LSF by

$$\hat{\mathcal{P}}_a[l;n] = \frac{1}{M}\sum_{p=-M/2}^{M/2-1}\hat{\mathcal{C}}_a[l;n,p]. \tag{4}$$

Thresholds are applied to reduce the influence of measurement noise and the limited dynamic range on the calculation of the delay spread. The noise threshold is set to 5 dB and the sensitivity threshold is set to 30 dB [12].

B. Pathloss Coefficient

To obtain the path loss coefficients we calculate the received power for each stationarity region l and antenna a by

$$\hat{\mathcal{P}}_a[l] = \sum_{n=0}^{Q-1}\hat{\mathcal{P}}_a[l;n] \tag{5}$$

Using the accurate positioning and timing information of the IMU, we associate each stationarity region with a distance d, i.e., $\mathrm{PL}_a(d) \sim \hat{\mathcal{P}}_a[l]$. We accumulate the path loss values of each antenna of all measurements runs and sort them by distance.

To obtain the pathloss coefficient we use a distance dependent path loss model for each antenna according to

$$\mathrm{PL}_a(d) = \mathrm{PL}_a(d_0) + 10n_a\log_{10}\left(\frac{d}{d_0}\right), \tag{6}$$

with $\mathrm{PL}_a(d_0)$ the path loss at a reference distance d_0 and n_a the path loss coefficient of antenna a. We use a two-slope model, since the measurement consists of an LOS and an NLOS part [1], where we split the model at the transition between LOS to NLOS.

We use a two-dimensional least squares (LS) fitting where we calculate $\mathrm{PL}_a(d_0)$ and n_a for each antenna such that the mean square error (MSE) between model and measurement data is minimized. The respective path loss coefficients are then obtained by averaging over the path loss coefficients within the respective frequency bands, i.e., $\bar{n} = \frac{1}{A}\sum_{a=1}^{A} n_a$.

C. Channel Hardening

We consider an uplink massive MIMO system where one user is transmitting to a base station (BS) deploying A antennas. We construct the channel vector at symbol index m by assembling the coherently measured and sampled channel transfer function $\hat{H}_a[m,q]$

$$\mathbf{h}_m = \left[\hat{H}_0[m],\hat{H}_1[m],\ldots,\hat{H}_{A-1}\right]^\mathrm{T} \in \mathbb{C}^{A\times 1}. \tag{7}$$

The subcarrier index q is dropped for simplicity, as all following analysis only considers one subcarrier at a time.

By applying the beamforming vector $\mathbf{w}_m \in \mathbb{C}^{A\times 1}$ in the uplink the received uplink symbol is

$$y_m = \mathbf{w}_m^\mathrm{H}\mathbf{h}_m x_m + z_m \tag{8}$$

with x_m the transmit symbol at time instant m and $z_m \underset{i.i.d}{\sim} \mathcal{CN}\left(0,\sigma^2\right)$.

The large number of antennas $A \gg K \gg 1$ leads to linear beam-forming being close to optimal. Additionally, the law of large numbers guarantees that the effective channel $\mathbf{w}_m^\mathrm{H}\mathbf{h}_m$ becomes quasi-deterministic – a process called *channel hardening* [17]. As a measure for channel hardening, we revert to the signal component's ratio of the standard deviation estimation to its estimated mean over M consecutive time indices [17]

$$\gamma_l = \frac{\sqrt{\frac{1}{M-1}\sum_{m=-M/2+lM}^{M/2-1+lM}\left(\left|\mathbf{w}_m^\mathrm{H}\mathbf{h}_m\right|^2-\mu_l\right)^2}}{\mu_l}, \tag{9}$$

$$\mu_l = \frac{1}{M}\sum_{m=-M/2+lM}^{M/2-1+lM}\left|\mathbf{w}_m^\mathrm{H}\mathbf{h}_m\right|^2, \tag{10}$$

which tends to zero as the channel becomes more and more deterministic. We consider in what follows the beam-forming vector $\mathbf{w}_m$ to being calculated via the maximum ratio combining (MRC) approach, i.e., $\mathbf{w}_m = \mathbf{h}_m$.

IV. Result Discussion

A. Delay Spread

Figures 4 and 5 show the delay spread averaged over antennas, 24 antennas for the 1890 MHz band and 8 antennas for the 748 MHz band, plotted versus distance. We observe that we obtain approximately the same average delay spread for each measurement run within one frequency band. The delay spread for 748 MHz is slightly smaller since in this case a stronger LOS path is present. The increase in delay spread at larger distances in the 1890 MHz band can be explained by a weaker LOS component.

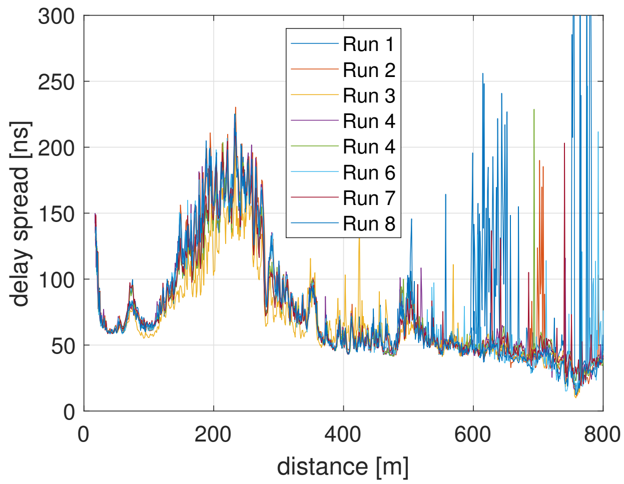

Fig. 4. RMS delay spread vs. distance for all 8 measurement runs for the 1890 MHz band.

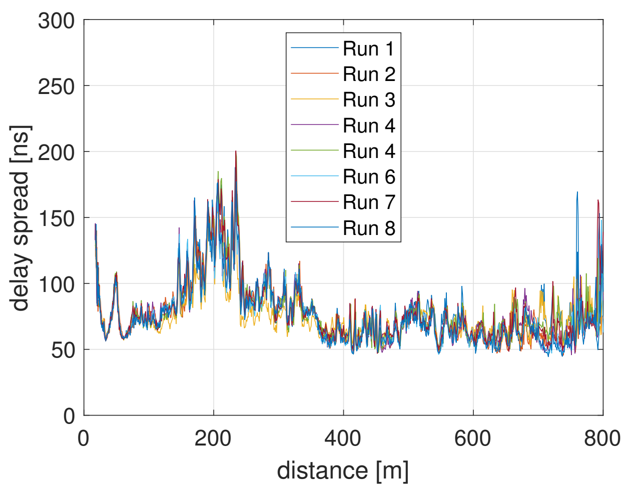

Fig. 5. RMS delay spread vs. distance for all 8 measurement runs for the 748 MHz band.

B. Pathloss Coefficient

Figure 6 shows the path loss versus the logarithmic distance of antenna 4 (1890 MHz) and 26 (748 MHz), respectively. We split the plot into two regions a) LOS from 60 m to 470 m b) and NLOS from 470 m to 800 m. As the locomotive moves from LOS to NLOS we observe a path loss increase of around 8 dB in the 1890 MHz band, while we observe a 4 dB path loss increase at the 748 MHz frequency band, originating from better diffraction around the corner of the railway museum.

From the LS fit described in Section III-B we obtain a pathloss coefficient of $n_{\text{LOS-1890 MHz}} = 1.81$ and $n_{\text{LOS-748 MHz}} = 2.2$ for the LOS case and $n_{\text{NLOS-1890 MHz}} = 5.15$ and $n_{\text{NLOS-748 MHz}} = 6.21$ for the NLOS case.

C. Channel Hardening

For the channel hardening evaluation we consider a maximum distance of 470 m from the bridge. To obtain a better

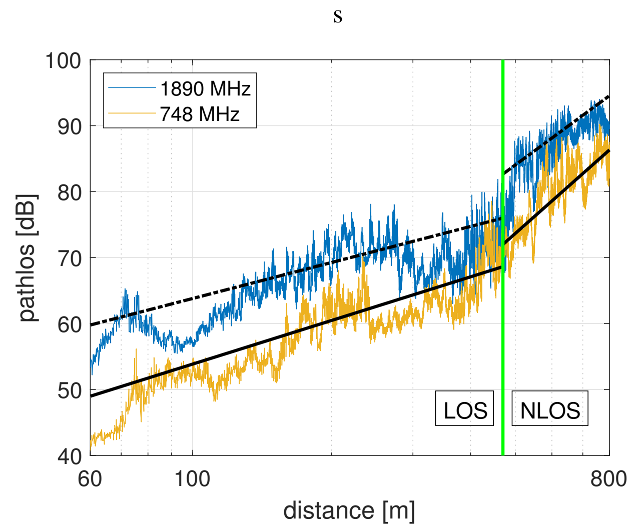

Fig. 6. Pathloss vs. distance for 1890 MHz (antenna 4, blue) and 748 MHz (antnna 26, yellow). LOS changes to NLOS at a distance of approx. 470 m.

statistic we evaluate a) γ_l at each subcarrier q and use a stacked vector of all subcarrieres for evaluation and b) use all 8 measurement runs.

In Fig. 7 we show the channel hardening cumulative distribution functions (CDFs) for the 1890 MHz band for an increasing number of antennas. The antennas are taken from the same ULA row for up to 12 antennas. We observe that increasing the number of antennas in azimuth leads to better channel hardening. An additional ULA row of antennas in elevation, however, does have a negligible effect on channel hardening in this measurement. A similar result can be observed for the 748 MHz band, shown in Fig. 8. Finally, the comparison of the frequency bands in Fig. 9 shows, that lower frequency bands allow for better channel hardening.

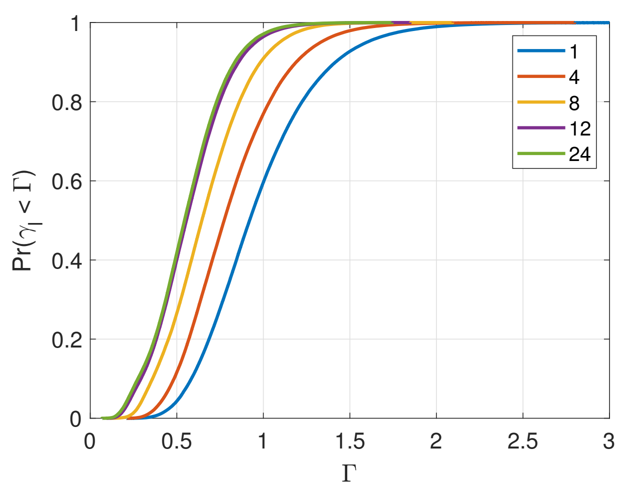

Fig. 7. Channel hardening vs. number of antennas for LOS for 1890 MHz calculated over all measurement runs. Adding antennas in elevation does not significantly change channel hardening.

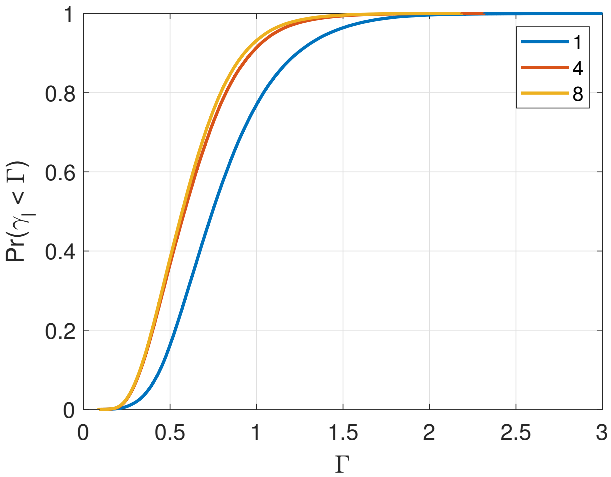

Fig. 8. Channel hardening vs. number of antennas for LOS for 748 MHz calculated over all measurement runs.

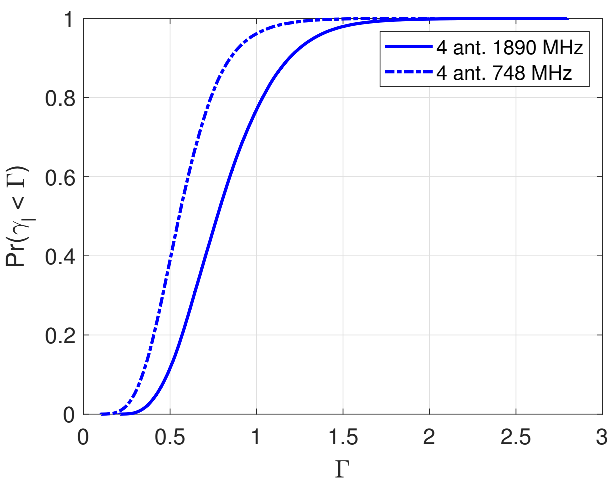

Fig. 9. Comparison of channel hardening for LOS between 748 MHz and 1890 MHz calculated over all measurement runs. The plots indicate better channel hardening at lower frequency bands.

V. Conclusion

In this paper we presented the results of a massive MIMO dualband measurement campaign for a railway station scenario, where a locomotive moved from LOS to NLOS. We analyzed the path loss coefficients, RMS delay spread and the channel hardening coefficients. In the LOS case we obtain path loss coefficients close to 2 in the NLOS case area we obtain coefficients from 5-6. The measurements show that the RMS delay spread at lower frequencies is slightly smaller compared to higher frequencies, due to a stronger LOS component at lower frequencies. Finally, the results show that increasing the number of receive antennas in vertical domain, does not allow for better channel hardening and that lower frequencies allow for better channel hardening with the same amount of antennas.

Acknowledgment

The project TARO is funded by the “Austrian Federal Ministry of Climate Action, Environment, Energy, Mobility, Innovation and Technology (BMK)” and “The Austrian Research Promotion Agency (FFG)” and the project DEDICATE (Principal Scientist grant) at the AIT Austrian Institute of Technology.

References

[1] P. Unterhuber, M. Walter, U.-C. Fiebig, and T. Kürner, “Stochastic channel parameters for train-to-train communications,” *IEEE Open Journal of Antennas and Propagation*, vol. 2, pp. 778–792, 2021.

[2] C.-X. Wang, A. Ghazal, B. Ai, Y. Liu, and P. Fan, “Channel measurements and models for high-speed train communication systems: A survey,” *IEEE Communications Surveys and Tutorials*, vol. 18, no. 2, pp. 974–987, 2016.

[3] S. Zelenbaba, L. W. Mayer, E. Mozo, F. Wirth, R. Hladik, A. A. Gómez, L. Bernadó, M. Schiefer, and T. Zemen, “Characterization of time-variant wireless channels in railway communication scenarios,” in *2019 IEEE 2nd 5G World Forum (5GWF)*, 2019, pp. 536–541.

[4] B. Ai, A. F. Molisch, M. Rupp, and Z.-D. Zhong, “5G key technologies for smart railways,” *Proceedings of the IEEE*, vol. 108, no. 6, pp. 856–893, 2020.

[5] S. Li, Y. Liu, L. Lin, and Q. Sun, “Measurements and characterization for millimeter-wave massive MIMO channel in high-speed railway station environment at 28 GHz,” *International Journal of Antennas and Propagation*, vol. 2021, p. 4580506, Oct 2021. [Online]. Available: https://doi.org/10.1155/2021/4580506

[6] M. Hofer, D. Löschenbrand, J. Blumenstein, H. Groll, S. Zelenbaba, B. Rainer, L. Bernadó, J. Vychodil, T. Mikulasek, E. Zöchmann, S. Sangodoyin, H. Hammoud, B. Schrenk, R. Langwieser, S. Pratschner, A. Prokes, A. F. Molisch, C. F. Mecklenbräuker, and T. Zemen, “Wireless vehicular multiband measurements in centimeterwave and millimeterwave bands,” in *2021 IEEE 32nd Annual International Symposium on Personal, Indoor and Mobile Radio Communications (PIMRC)*, 2021, pp. 836–841.

[7] D. Löschenbrand, M. Hofer, L. Bernadó, G. Humer, B. Schrenk, S. Zelenbaba, and T. Zemen, “Distributed massive MIMO channel measurements in urban vehicular scenario,” in *2019 13th European Conference on Antennas and Propagation (EuCAP)*, 2019, pp. 1–5.

[8] S. Zelenbaba, M. Hofer, D. Löschenbrand, G. Kail, M. Schiefer, and T. Zemen, “Spatial properties of industrial wireless ultra-reliable low-latency communication MIMO links,” in *2019 53rd Asilomar Conference on Signals, Systems, and Computers*, 2019, pp. 1054–1058.

[9] M. Friese, “Multitone signals with low crest factor,” *IEEE Transactions on Communications*, vol. 45, no. 10, pp. 1338–1344, 1997.

[10] D. Löschenbrand, M. Hofer, L. Bernadó, S. Zelenbaba, and T. Zemen, “Towards cell-free massive MIMO: A measurement-based analysis,” *IEEE Access*, pp. 89 232–89 247, 2022.

[11] Accessed: 2022-06-30. [Online]. Available: https://www.ptsyst.com/

[12] L. Bernadó, T. Zemen, F. Tufvesson, A. F. Molisch, and C. F. Mecklenbrauker, “Delay and Doppler spreads of nonstationary vehicular channels for safety-relevant scenarios,” *IEEE Trans. Veh. Technol.*, vol. 63, no. 1, pp. 82–93, Jan. 2014.

[13] G. Matz, “On non-wssus wireless fading channels,” *IEEE Trans. Wireless Commun.*, vol. 4, no. 5, pp. 2465–2478, Sep. 2005.

[14] M. Hofer, D. Löschenbrand, S. Zelenbaba, A. Dakić, B. Rainer, and T. Zemen, “Wireless 3 GHz and 30 GHz vehicle-to-vehicle measurements in an urban street scenario,” in *2022 IEEE 96th Vehicular Technology Conference (VTC2022-Fall)*, 2022 - to be presented, pp. 1–5.

[15] D. Slepian, “Prolate spheroidal wave functions, Fourier analysis, and uncertainty-V: The discrete case,” *Bell Syst. Techn J.*, vol. 57, no. 5, pp. 1371–1430, May 1978.

[16] E. Zöchmann, M. Hofer, M. Lerch, S. Pratschner, L. Bernadó, J. Blumenstein, S. Caban, S. Sangodoyin, H. Groll, T. Zemen, A. Prokeš, M. Rupp, A. F. Molisch, and C. F. Mecklenbräuker, “Position-specific statistics of 60 GHz vehicular channels during overtaking,” *IEEE Access*, vol. 7, pp. 14 216–14 232, 2019.

[17] T. Zemen, D. Löschenbrand, M. Hofer, C. Pacher, and B. Rainer, “Orthogonally precoded massive MIMO for high mobility scenarios,” *IEEE Access*, vol. 7, pp. 132 979–132 990, 2019.